View metadata, citation and similar papers at core.ac.uk

brought to you by CORE

provided by Wageningen University & Research Publications

Statistical thermodynamics of association colloids. I. Lipid bilayer membranes

F. A. M. Leermakers and J. M. H. M. Scheutjens

Citation: J. Chem. Phys. **89**, 3264 (1988); doi: 10.1063/1.454931
View online: http://dx.doi.org/10.1063/1.454931
View Table of Contents: http://jcp.aip.org/resource/1/JCPSA6/v89/i5
Published by the American Institute of Physics.

Additional information on J. Chem. Phys.

Journal Homepage: http://jcp.aip.org/
Journal Information: http://jcp.aip.org/about/about_the_journal
Top downloads: http://jcp.aip.org/features/most_downloaded
Information for Authors: http://jcp.aip.org/authors

ADVERTISEMENT

Downloaded 28 Feb 2012 to 137.224.252.10. Redistribution subject to AIP license or copyright; see http://jcp.aip.org/about/rights_and_permissions

Statistical thermodynamics of association colloids. I. Lipid bilayer membranes

F. A. M. Leermakers and J. M. H. M. Scheutjens
Department of Physical and Colloid Chemistry, Agricultural University Wageningen, Dreijenplein 6, 6703 HB Wageningen, The Netherlands

(Received 28 March 1988; accepted 20 May 1988)

Step-weighted random walks (modified Markov chain statistics) combined with a self-consistent-field approximation form the basic concepts of a Flory–Huggins-type of theory to describe the lipid bilayer.[1] The purpose of the present paper is to extend this model by incorporating the rotational isomeric state scheme, both for linear and branched chain molecules. Only three measurable interaction energy parameters of a Flory–Huggins-type are required, namely for the head group tail, the head group water, and the tail water contacts. In addition, the theory needs one energy parameter for the internal *trans/gauche* transition energy of the chain. Results of this self-consistent-field (SCF) theory are given for membranes formed by lecithin-like molecules. With respect to earlier work, more detailed insight is obtained in the behavior of the lipid bilayer above the gel to liquid phase transition temperature. Equilibrium conditions are formulated. Segment density profiles and solvent distributions are calculated. It is shown that the two apolar tails of the lecithin do not behave identically. The tail next to the head group is lifted slightly more out of the membrane than the other tail. The well-known balance of forces, responsible for membrane formation is analyzed. We found that the repulsive tail head interaction, often ignored in theories, is essential for the stability of association colloids.

INTRODUCTION

Lipid bilayer membranes provide the living cell with a surface on which protein molecules have interaction. Membranes also are the interfaces between cell compartments. The recognition that these properties serve vital functions in living material has stimulated the research on lipid bilayers. There is a need for a general theory which describes equilibrium properties of lipid bilayers, explains the polymorphism of lipid aggregates, gives insight into the molecular behavior of the lipids in an aggregate, and eventually shows the gel to liquid phase transition behavior. These topics have been the subject of many studies and several theories deal with various aspects of this problem. In a series of papers we will show that it is possible to design a comprehensive statistical thermodynamical theory which is able to deal with all of these aspects simultaneously.

Molecular dynamics (MD) is an alternative method to obtain detailed information on aggregates of amphipolar molecules. One of the first MD studies on the bilayer membrane is performed by Van der Ploeg and Berendsen.[2] The excluded volume of the molecules is treated rigorously and all interactions are taken into account with high accuracy. Indeed, modern simulations do not fix the head groups positions to a certain plane and the few results obtained so far seem realistic.[3] Unfortunately, MD needs many parameters. It has been shown recently that results depend on the model which is used to simulate the solvent phase.[4] Further, the method is limited by the small number of molecules, and the relatively short tail lengths, which can be taken into account. Because of the time scale of the simulations (in the order of 100 ps) a slow process like the exchange of lipids between a membrane and the bulk solution cannot yet be simulated by molecular dynamics.

In principle, Monte Carlo (MC) simulations may also be useful to gain insight into the behavior of amphipolar molecules in aqueous media. Results for small surfactant molecules have recently been obtained by Owenson and Pratt.[5] They did not restrict the positions of the head groups, and therefore their results should compare well with ours. However, for computational reasons, detailed information on lipid membranes formed by lecithins is not yet available.

Statistical mechanical calculations based on a self-consistent field do not rely as much on computer capacity as MD or MC techniques do. The quality of the outcome of such calculations depends on the rigor of the partition function derived. Several groups studied the conformations of hydrocarbon tails anchored to a given plane[6,7] or have used arbitrary head group positions.[8] The main result of these theories is the order profile along the hydrocarbon chain. Very critical for this profile is the effective head group area or, in other words, the number of chains per surface area. This parameter can be estimated from experimental values of the membrane thickness. The question why a given membrane thickness is found remains to be solved.

Our theory has a more *ab initio* character. It allows all molecules to be distributed freely throughout the system. In this way, equilibrium with the bulk solution is automatically guaranteed. In other words, the membrane structure can no longer be dictated. The membrane thickness and the average surface area per molecule are results of the calculations. The composition of the molecules and the values for the interaction parameters determine the properties of the aggregates. The morphology of the association colloids can also be stud-

 0021-9606/88/173264-11$02.10 © 1988 American Institute of Physics

Downloaded 28 Feb 2012 to 137.224.252.10. Redistribution subject to AIP license or copyright; see http://jcp.aip.org/about/rights_and_permissions

ied if one allows for nonplanar aggregates as well.

This article explains the statistical and computational aspects of the rotational isomeric state scheme in a Markov approximation, applied to branched molecules in a lamellar geometry. All conformations of a chain are generated in the mean field due to all of the other chains. During this generating process the different conformations are properly weighted. Our method of generating chain conformations shows similarities with the theory of Dill and co-workers.[8] After some manipulations the segment density profile is found. The statistical weight of each individual conformation can be calculated when this profile is known. Therefore, the theory can also be formulated in terms of a set of conformations defining the equilibrium properties of the system.[9] When doing so, the relation between our theory and MC simulations,[5] or with theories in which the individual (tail) conformations are generated, as in the work of Gruen,[7] is more clear. From this set of chain conformations, the partition function of the system can be calculated from which all necessary thermodynamic quantities follow. For more details of the derivation of the partition function, we refer to other papers.[1,10]

FIRST ORDER MARKOV CHAINS

A polymer chain is built up of r segments (e.g., CH_2 groups), with ranking numbers $s = 1,...,r$. Each segment may be connected to one or more other segments in the chain, but we assume that no ring structures are present, so that each chemical bond connects two independent parts of the chain. One of the main goals of a many-chain problem is to calculate the whole set of conformations of all molecules in a given volume. To deal with this, it is convenient to design a lattice composed of lattice sites to which polymer segments or solvent molecules are confined. Scheutjens and Fleer modified a matrix method first introduced by Di Marzio and Rubin[11] to generate all conformations of the polymer chains in this lattice. In the absence of a potential field, this matrix formalism can be shown to be equivalent with random walk statistics. It is characteristic for the random walk on the lattice that each step has Z options, irrespective of previous steps where Z is the coordination number of the lattice, i.e., the number of neighboring lattice sites. In the present elaboration the lattice consists of parallel layers of L lattice sites each. They are numbered $z = 1,...,M$, where layer numbers 1 and M form the boundaries of the system. A fraction λ_{-1} of these Z sites is situated in a previous layer, a fraction λ_1 in the next layer, and a fraction λ_0 in the same layer. We are interested in the density distribution of each segment for a given potential profile $u(z)$ (a free energy per segment). This profile is usually different for each type of segment or solvent molecule and includes hard core interactions and specific contact energies. In this way we can use a simple Boltzmann statistics to obtain the distribution functions. For example, the density distribution of solvent, denoted by subscript W, is given by

$$\phi_W(z) = \phi_W^b G_W(z), \tag{1}$$

where $\phi_W(z)$ is the volume fraction of solvent in layer z, ϕ_W^b that in the bulk solution, and $G_W(z) = \exp[-u_W(z)/kT]$ gives the distribution function of solvent molecules. Similarly, $G_A(z) = \exp[-u_A(z)/kT]$ gives the distribution function of monomers of type A in a potential field $u_A(z)$, whereas $G_A(z)\lambda_{z'-z}G_B(z')$ gives the distribution function of AB dimers, where segment A is in layer z and segment B in layer z'. The distribution of A segments of these dimers is thus given by $G(z,A_B) = G_A(z)\Sigma_{z'}\lambda_{z'-z}G_B(z')$.

Generally, each segment s contributes a factor $G_i(z,s)$ to the distribution function of a chain i and the distribution function of the last segment of a chain of s segments can be expressed in a Markov approximation

$$G(z,s_1) = G(z,s)\sum_{z'} \lambda_{z'-z} G(z',s_1'). \tag{2}$$

The subscript 1 refers to the bond 1 with which the rest of the chain is connected. Note that the subindex i is dropped to indicate that the equation is general applicable. $G(z',s_1')$ is the distribution function of segment s' when the bond between s and s' is disconnected. In shorthand notation Eq. (2) is written as

$$G(z,s_1) = G(z,s)\langle G(z,s_1')\rangle. \tag{3}$$

The angular brackets denote a weighted averaging of $G(z,s_1')$ over layers $z-1$, z, and $z+1$. Equation (3) is a recurrence relation that expresses the end segment distribution in terms of that of a chain that is one segment shorter. A segment with chain parts at two of its bonds (1 and 2) has a distribution function $G(z,s_{12}) = \langle G(z,s_1')\rangle G(z,s)\langle G(z,s_2'')\rangle$ or

$$G(z,s_{12}) = G(z,s_1)G(z,s_2)/G(z,s). \tag{4}$$

We have assumed that segment s' and s'' may overlap each other occasionally (Markov-type behavior). The volume fraction of segment s in layer z is now calculated as

$$\phi(z,s_{12}) = CG(z,s_{12}), \tag{5}$$

where C is a normalization constant, obtained from the volume fraction ϕ^b:

$$C = \frac{\phi^b}{r} \tag{6}$$

or from the total amount of segments $\theta = \Sigma_z\Sigma_s\phi(z,s)$ in the system. Since $\Sigma_z G(z,s_{12})$ is independent of s, $\Sigma_s\Sigma_z G(z,s_{12}) = r\Sigma_z G(z,r_1) = r\ G(r_1)$, the normalization constant is

$$C = \frac{\theta}{r\ G(r_1)}. \tag{7}$$

Starting at either chain end, Eq. (3) generates all end segment distribution functions needed in Eq. (4) from the monomer distribution functions $G(z,s)$ [substituted by $G_A(z)$, $G_B(z)$, etc., depending on the type of segment s], so that the volume fraction distributions can be obtained from Eq. (5). This procedure is repeated for each type of molecule (i) in the system. For monomers Eq. (5) reduces to the simple form of Eq. (1).

In each layer z the total volume fractions of solvent and segments should obey the volume restriction requirement:

$$\Sigma_x \phi_x(z) = 1. \tag{8}$$

Here, x denotes segment or solvent type (x = A,B,W,...). In

Downloaded 28 Feb 2012 to 137.224.252.10. Redistribution subject to AIP license or copyright; see http://jcp.aip.org/about/rights_and_permissions

the simplest case there are only hard core interactions in the system, so that $G_x(z) = \exp[-u'(z)/kT]$ for all segment types x. In this case $u'(z)$ is the hard core potential and is chosen such that Eq. (8) is satisfied. More generally, the potential profile of segment x includes energetic contributions from nearest neighbor interactions, which can be expressed in terms of Flory–Huggins parameters χ_{xy}:

$$u_x(z) = u'(z) + kT\Sigma_y\chi_{xy}(\langle\phi_y(z)\rangle - \phi_y^b). \quad (9)$$

The summation y runs over all segment and solvent types. The angular brackets again indicate a weighted average over three consecutive layers ($z' = z-1, z, z+1$):

$$\langle\phi(z)\rangle = \Sigma_{z'}\lambda_{z'-z}\phi(z'). \quad (10)$$

The number of equations [Eqs. (8) and (9)] always equals the number of unknowns [$u'(z)$ and $u_x(z)$], so that the set of simultaneous equations can be solved numerically.

Branched molecules are treated very similarly. If segment s (connected with bonds 1 and 2 in the chain) has a branch at bond 3, we apply Eq. (4) to connect the chain parts at bonds 1 and 2 and an equivalent Eq. (11) to connect the branch at bond 3:

$$G(z,s_{123}) = G(z,s_{12})G(z,s_3)/G(z,s). \quad (11)$$

$G(z,s_3)$ is generated using Eq. (3) and starting at the end of the branch chain. The density distribution of the branching segment follows from $\phi(z,s_{123}) = CG(z,s_{123})$. Equations (4) and (5) remain valid for all other segments, because these segments have only two bonds each. However, $G(z,s_1)$ or $G(z,s_2)$ should include the contribution of the branch. If the branch is in the chain part that is connected to bond 1 of segment s and the branch point is s', we can obtain $G(z,s_1)$ using Eq. (3) starting at $G(z,s'_{13})$: $G(z,s''_1) = G(z,s'')\langle G(z,s'_{13})\rangle$, where s'' is the segment directly connected to s'.

ROTATIONAL ISOMERIC STATE SCHEME

Due to steric hindrance, a sequence of three C–C bonds has three favorable, one *trans* (t) and two *gauche* (g^+,g^-), configurations (see Fig. 1). The two *gauche* configurations have an energy $U^g \approx 1\ kT$ higher than the *trans* configuration. Each additional C–C bond has, again, three possible orientations which form *trans* or *gauche* configurations with its two predecessors. The whole chain will fit on a tetrahedral (diamond) lattice, where each bond is in one of four orientations e'', f'', g'', or h''. In each of these orientations we distinguish two opposite directions: e and e', f and f', g and g', h and h', respectively (see Fig. 2). We orient the lattice in such a way that bonds in orientations f'' and g'' connect segments within the same lattice layer and bonds in orientations e'' and h'' connect segments in neighboring lattice layers. If we rotate this lattice around its z axis over angles of 120° we get a superposition of 3 tetrahedral lattices which is very similar to a hexagonal lattice: each lattice site gets 12 instead of 4 neighbors, but the 6 of them in the same layer do not form a hexagon. As we will apply a mean field approximation within each layer, this difference will not affect the results. Hence it will suffice to consider only the tetrahedral lattice with the four bond orientations defined above.

There are two types of sites in the lattice which are mirror images of each other. Sites of type I have neighbors (all of type II) in directions e, f, g, and h, whereas sites of type II are surrounded by sites of type I in directions e', f', g', and h' [see Fig. 2(b)]. We will assume that a segment can at the most have four possible bonds. These bonds give a segment an orientation, irrespective of whether the bonds are free or not. A segment on a site in a tetrahedral lattice may assume one out of 12 orientations: 1 bond can choose between 4 directions and a second bond between 3. The directions of any other bonds are then fixed because of its stereo specificity. The first column of Table I lists all these orientations for a site of type I. Each orientation can be obtained from another

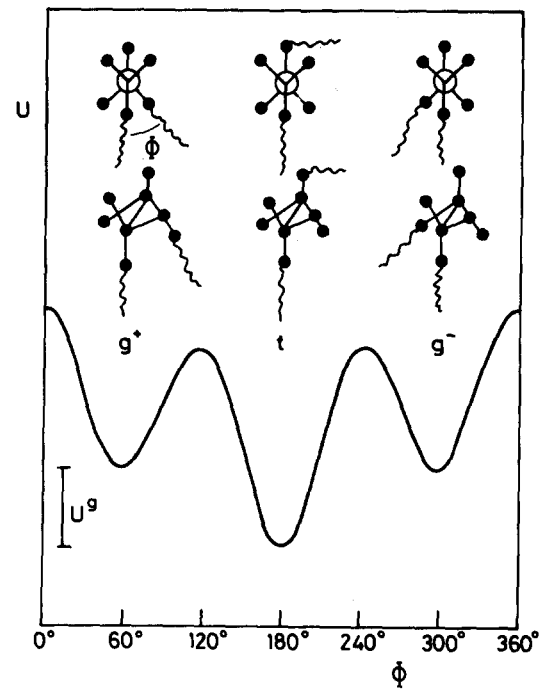

FIG. 1. Schematic drawing of *gauche* and *trans* configurations in a chain and the energy as a function of the angle Φ between two consecutive bonds in the chain. The three minima in the energy curve correspond with a g^+, t, and g^- configuration, respectively. The *trans* configuration is energetically most favorable.

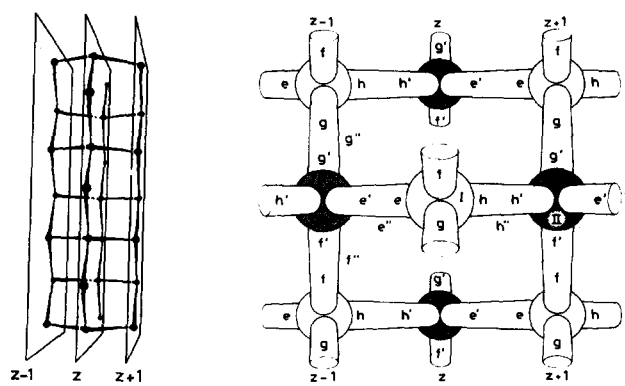

FIG. 2. (a) Identification of lamellae in a tetrahedral lattice. All segments are on one of the parallel planes. (b) Alternative representation of the same lattice. The eight bond directions, four bond orientations, and the two types of sites are indicated.

Downloaded 28 Feb 2012 to 137.224.252.10. Redistribution subject to AIP license or copyright; see http://jcp.aip.org/about/rights_and_permissions

TABLE I. Compilation of segment orientations in a tetrahedral lattice.

Segment	Isomer I		Isomer II	
Site	I	II	I	II
Bond number	1234	1 2 3 4	1234	1 2 3 4
Orientation	*ehfg*	*h'e'f'g'*	*hefg*	*e'h'f'g'*
	efgh	*h'f'g'e'*	*hfge*	*e'f'g'h'*
	eghf	*h'g'e'f'*	*hgef*	*e'g'h'f'*
	fhge	*f'e'g'h'*	*fegh*	*f'h'g'e'*
	fgeh	*f'g'h'e'*	*fghe*	*f'g'e'h'*
	fehg	*f'h'e'g'*	*fheg*	*f'e'h'g'*
	gefh	*g'h'f'e'*	*ghfe*	*g'e'f'h'*
	gfhe	*g'f'e'h'*	*gfeh*	*g'f'h'e'*
	ghef	*g'e'h'f'*	*gehf*	*g'h'e'f'*
	hgfe	*e'g'f'h'*	*egfh*	*h'g'f'e'*
	hfeg	*e'f'h'g'*	*efhg*	*h'f'e'g'*
	hegf	*e'h'g'f'*	*ehgf*	*h'e'g'f'*

one by rotation around one of the bonds (keep any one bond in position and exchange the three others). The stereo isomer is obtained by exchanging any two bond orientations. The third column of Table I lists all orientations of the isomer on a site of type I (exchanging h and e). As a mirror image of a segment on a site I is equivalent to its stereo isomer on a site II, we obtain a complete list of bond direction combinations on sites II by reversing all directions in the first and third column in Table I, giving columns four and two, respectively.

A segment orientation is defined by specifying the directions of two of its bonds. We will use the symbol s^{ef} when the first bond of segment s is in direction e and the second bond in direction f. Equivalently, $s^{g'\cdot h'}$ signifies that bond one is in direction g' and bond three is in direction h'. To indicate the fact that the segment is part of a chain we write $s_{14}^{h'\cdots e'}$ if bond 1 in direction h' and bond 4 in direction e' are connected to other chain parts.

In this paper we assume that the potential profile [Eq. (9)] is independent of the orientation of a segment, so that

$$G(z,s^{\alpha\beta}) = \begin{cases} 0, & \text{if } \alpha=\beta \\ G(z,s), & \text{otherwise} \end{cases}, \tag{12}$$

where α and β stand for the bond directions e, f, g, and h (or e', f', g', and h' for sites of type II). There are 24 nonzero independent values $G(z,s^{\alpha\beta})$. Equation (2), describing elongation of the chain at s' by one segment s, becomes

$$G(z,s_1^{\alpha\beta}) = G(z,s^{\alpha\beta}) \sum_{\gamma'} \lambda^{\beta''-\alpha''-\gamma''} G(z',s_1'^{\gamma'\alpha'}). \tag{2a}$$

In this case bond 1 of segment s (in direction α) is connected to bond 2 of segment s' (in direction α'). Layer z' is either $z-1, z$, or $z+1$, depending on the direction of α'. There are only three nonzero contributions to $G(z,s_1^{\alpha\beta})$, because all combinations with $\alpha=\beta$ are excluded by Eq. (12). The superscript $\beta''-\alpha''-\gamma''$ refers to a sequence of three bonds, in orientation β'', α'', and γ'', respectively (a superscript $\beta''\alpha''\gamma''$ would refer to three bond orientations of the same segment), forming a *gauche* or *trans* configuration. The three configurations are properly weighted by λ^t or λ^g:

$$\lambda^{\alpha''-\beta''-\gamma''} = \begin{cases} \lambda^t, & \text{if } \alpha''=\gamma'' \\ \lambda^g, & \text{otherwise} \end{cases}, \tag{13}$$

where $\lambda^g = 1/[2+\exp(U^g/kT)]$ and $\lambda^t = 1-2\lambda^g$. Equation (2a) applies even to dimers and end segments, because the difference between t and g affects only the orientation of the next bond, which is a free bond in these cases. Therefore, the recurrence equation (2a) can be started at $G(z,s_1^{\alpha\beta}) = G(z,s^{\alpha\beta})$. The equivalent of Eq. (2a), starting at the other chain end reads

$$G(z,s_2^{\alpha\beta}) = G(z,s^{\alpha\beta}) \sum_{\gamma'} \lambda^{\alpha''-\beta''-\gamma''} G(z',s_2'^{\beta'\gamma'}),$$

where bond 2 of segment s in direction β is attached to bond 1 of segment s' in direction β'.

The end-to-end connection of two chains at segment s in orientation $\alpha\beta$ is now just a variation of Eq. (4), because all *gauche* and *trans* energies are already accounted for:

$$G(z,s_{12}^{\alpha\beta}) = G(z,s_1^{\alpha\beta})G(z,s_2^{\alpha\beta})/G(z,s^{\alpha\beta}) \tag{4a}$$

and $G(z,s_{12})$ in Eq. (5) becomes the average value of $G(z,s_{12}^{\alpha\beta})$:

$$G(z,s_{12}) = \sum_{\alpha}\sum_{\beta} \lambda^{\alpha\beta} G(z,s_{12}^{\alpha\beta}). \tag{14}$$

Here, $\lambda^{\alpha\beta} = 1/24$ is the inverse of the number of segment orientations on sites of type I and II. The number of segments on sites of type I must be equal to those on type II $\Sigma_i \phi_i(z_{\mathrm{I}}) = \Sigma_i \phi_i(z_{\mathrm{II}}) = 0.5$. In the present treatment there is no numerical difference between $G(z,s^{\alpha\beta})$ and $G(z,s^{\alpha'\beta'})$, so that this constraint is automatically obeyed. Moreover, the consecutive segments in a chain are placed on alternate type of sites. Only the chain as a whole may in certain systems prefer to start always on the same type of site, e.g., in a crystal the chains would be all in the same orientation.

A branch in the chain presents some extra difficulties. Instead of Eq. (11) we have

$$G(z,s_{123}^{\alpha\beta\gamma}) = G(z,s_1^{\alpha\beta\gamma})G(z,s_2^{\alpha\beta\gamma})G(z,s_3^{\alpha\beta\gamma})/G(z,s^{\alpha\beta\gamma})^2. \tag{11a}$$

Although the orientation of a segment is fixed by the direction of two of its bonds, all three bond directions are indicated in Eq. (11a) for the sake of clearness. Obviously, $G(z,s^{\alpha\beta\gamma}) = G(z,s^{\alpha\beta})$. The chain end distribution function $G(z,s_1^{\alpha\beta\gamma})$ indicates that the rest of the chain is connected to bond 1 of s, which is in the α direction. This quantity is found by a modification of Eq. (2a). When s' is the segment adjacent to the branching segment s then

$$G(z,s_1^{\alpha\beta\delta}) = G(z,s^{\alpha\beta\delta}) \sum_{\gamma} \lambda^{\gamma''-\alpha''-\beta''\delta''} G(z',s_1'^{\gamma'\alpha'}), \tag{2b}$$

where bond 2 of segment s' in direction α' is connected to bond 1 of s in direction α. To segment s also the directions β and δ are assigned to which bond 2 and 3 will be connected, respectively. The parameter $\lambda^{\gamma''-\alpha''-\beta''\delta''}$ weights their contributions:

$$\lambda^{\alpha''-\beta''-\gamma''\delta''} = \begin{cases} \lambda^{tg}, & \text{if } \alpha''=\gamma'' \text{ or } \alpha''=\delta'' \\ \lambda^{gg}, & \text{otherwise} \end{cases}, \tag{15}$$

where $\lambda^{tg} = \lambda^t\lambda^g/(2\lambda^t\lambda^g + \lambda^g\lambda^g)$ and $\lambda^{gg} = 1-2\lambda^{tg}$. It is illustrative to give the equivalent expression (2b) for the case that bond 3 of s' in direction β' is connected to bond 2 of segment s, while bond 1 and 3 of segment s are in directions α

Downloaded 28 Feb 2012 to 137.224.252.10. Redistribution subject to AIP license or copyright; see http://jcp.aip.org/about/rights_and_permissions

and δ, respectively:

$$G(z,s_2^{\alpha\beta\delta}) = G(z,s^{\alpha\beta\delta}) \sum_{\gamma'} \lambda^{\gamma''-\beta''-\alpha''\delta''} G(z',s_2^{\gamma'\beta'}) .$$

Obviously, by the following equation a segment s'' in orientation $\alpha\beta$ is connected with bond 1 to bond 2 of segment s which has other chain parts at bonds 1 and 3:

$$G(z,s_1''^{\alpha\beta}) = G(z,s''^{\alpha\beta}) \sum_{\gamma'} \lambda^{\beta''-\alpha''-\gamma''\delta''} G(z',s_{13}^{\gamma'\alpha'\delta'}), \quad (2c)$$

where $G(z,s_{13}^{\alpha\beta\gamma}) = G(z,s_1^{\alpha\beta\gamma})G(z,s_3^{\alpha\beta\gamma})/G,(z,s^{\alpha\beta\gamma})$. The summation over γ' represents the three directions of bond 1 of segment s with bond 2 in direction α'. These orientations can be obtained from Table I and determine the directions δ' simultaneously. This formalism is easily extendible for a branch point with four groups. For example, a segment s'' in orientation $\alpha\beta$ is connected through bond 1 to bond 2 of segment s' to other chain parts at bonds 1, 3, and 4 by

$$G(z,s_1''^{\alpha\beta}) = G(z,s''^{\alpha\beta}) \sum_{\gamma'} \lambda^{\beta''-\alpha''-\gamma''\delta''\epsilon''} G(z',s_{134}^{\gamma'\alpha'\delta'\epsilon'}), \quad (2d)$$

where $\lambda^{\beta''-\alpha''-\gamma''\delta''\epsilon''} = \lambda^{ggt}/(3\lambda^{ggt}) = 1/3$.

COMPUTATIONAL ASPECTS

Due to the symmetry of the lattice and the mean field approximation, many of the quantities G are numerically equal. We have already mentioned the equivalence of sites of type I and II. Moreover, there will be an equal number of bonds in orientations e'' and h'' (between two layers) and similarly in orientations f'' and g'' (within a layer). Generally, for a segment with 2 bonds there are only 7 numerically different segment orientations $\alpha\beta$, instead of 24. These are listed in Table II. In Appendix A the resulting equations (2a) and (4a) are given in matrix notation.

For a segment with three or four bonds, each orientation on a site of type I has only one numerically equivalent orientation on a site of type II, e.g., $ehfg \equiv h'e'f'g'$, $efgh \equiv h'f'g'e'$, etc., so that 12 different numbers remain. (The corresponding pairs are listed in Table I next to each other.)

To fix the membrane on the lattice we place a reflecting boundary in the center of the bilayer[1] (there is no reason why the bilayer would be asymmetric), between layers 0 and 1. This is accomplished by setting all (image) quantities in layer $1-z$ equal to those in layer z. Thus, $G(1-z,s_{12}^{efgh}) = G(z,s_{12}^{hgfe})$, $\phi(1-z,s) = \phi(z,s)$, etc. In fact, the molecules are rotated over 180° rather than reflected, because a reflection would produce the stereo isomer. The rule to find the rotated bond directions is to replace e, f, g, h, e', f', g', and h' by h, g, f, e, h', g', f', and e', respectively.

Obviously, the reflecting boundary could also be placed in layer 0 so that quantities in layer $-z$ equal those in layer z. A similar reflecting boundary can be placed in the bulk solution, between layers M and $M+1$ or in layer M. Hence, calculations for only M or $M+1$ layers are to be performed. Membranes are initiated in the first few layers by a suitable initial guess (see Appendix B for numerical details).

TABLE II. Degenerate segment orientations.

$eh \equiv h'e'$
$ef \equiv eg \equiv h'g' \equiv h'f'$
$fh \equiv gh \equiv g'e' \equiv f'e'$
$fg \equiv gf \equiv g'f' \equiv f'g'$
$fe \equiv ge \equiv g'h' \equiv f'h'$
$hf \equiv hg \equiv e'g' \equiv e'f'$
$he \equiv e'h'$

EVALUATION OF THE MARKOV CHAIN AND MEAN FIELD APPROXIMATIONS

It is appropriate to summarize the shortcomings and advantages of the Markov chain approximation and, consequently, the local mean field approximation coupled to it. Strictly speaking, our chain statistics has pure Markov behavior only if all steps are weighted with a constant factor, i.e., for a homogeneous system. In a concentration gradient the steps are weighted according to the local potential and therefore our method may also be characterized as "a step weighted random walk." Since in a Markov approximation only short range correlations (along the chain) are taken care of, we were able to use a recurrent relation which guarantees (within certain limits) the generation of all allowed conformations of a chain in the average field of all other chains. By incorporation of some memory along the chain path (RIS scheme), direct backfolding can be forbidden. With this method we cannot prevent a chain segment to enter a lattice site which is already occupied by a segment of one of the other chains. We also allow the chain to enter a lattice site which is already occupied by a segment of the same chain if it is more than four bonds apart. We compensate for any multiple occupancy of sites by allowing only a total of L segments and solvent molecules in each lattice layer. The effect of this approach for the excluded volume is that the membrane thickness will be slightly underestimated.

The consequence of using the average segment density in each layer is that inhomogeneities in each layer parallel to the membrane are neglected. When a lamellar lattice is used, the membrane is forced to be flat and spontaneous undulations along the bilayer are not taken into account.

There are a few impressive achievements in the present treatment. One can generate all conformations of chains of up to 10 000 segments without too much computational effort. The segment density profiles of each conformation can be calculated so that very detailed information on the segment positions is available. Any number of different types of molecules (e.g., polydisperse polymers, additives, etc.) can be introduced without undue complications. If necessary, other interactions (e.g., electrostatic) or external potentials (e.g., long range van der Waals interactions) can be taken into account as well.

COMPARISON WITH OTHER THEORIES

Dill and co-workers use a different but similar recurrence relation to generate all possible conformations of chains on a lattice.[8] However, they fix the head groups in particular layers and allow all segments only to be in the

Downloaded 28 Feb 2012 to 137.224.252.10. Redistribution subject to AIP license or copyright; see http://jcp.aip.org/about/rights_and_permissions

same layer or in the layers closer to the center of the aggregates.

Gruen either samples the set of conformations, or generates the whole set.[7] His approach does not make use of a lattice and consequently his set of conformations for the lipid molecules is in this respect more realistic than ours. For computational reasons, a predetermined number of head groups were confined to a given layer so that equilibrium with the bulk solution was lost. A more severe drawback of his approach is that one cannot be sure to find the set of conformations which minimizes the free energy. Gruen generated several solutions obeying the space filling requirement. The chain packing corresponding to the lowest free energy found was accepted as the physical, realistic solution.

Both Gruen and Dill *et al.* did not allow solvent molecules or head groups in the tail region, and therefore they did not need to take energetic interactions into account. For the space filling requirement both theories need a kind of osmotic potential like our $u'(z)$.

In our theory all essential energetic interactions are accounted for. Our segment density profiles are self-consistent, and equilibrium with the bulk solution is always guaranteed. Standard thermodynamics are used to find the equilibrium properties of the system.

RESULTS AND DISCUSSION

Lipid molecules

We will concentrate on lecithin-like molecules modeled by a glycerol backbone, two identical tails of p (CH_2) apolar (A) segments each and a head group of q polar (B) segments:

$$\begin{array}{l} A_p - B - A \\ A_p - B - A \\ \qquad\quad\ \ A - B_q \end{array} \quad . \tag{16}$$

We disregard volume differences between a terminal CH_3 group and a CH_2 group, nor do we specify more details in the head group. Henceforth, the solvent simply is indicated as "water" and is modeled as a monomer of segment type W. The solvent molecules are denoted by $i = 1$ and the lipids by $i = 2$.

Interaction parameters

In the most simple case there are three χ parameters for the various contacts in the system. Roughly, χ_{AW} (tail segment/water interaction) is 1.6, χ_{BW} (head group segment/water interaction) is 0 or slightly negative, and χ_{AB} (tail segment/head group segment interaction) is around 1.5. This set of χ values implies that head groups are soluble in water, but the tails avoid head groups and water molecules (high χ values). It mimics the well-known opposing forces stabilizing the lipid aggregates. Phase separation between tails and water is the driving force for association. Head groups repel tails and therefore they are forced to be on the outside of the aggregate. As they like water, micelle or membrane growth is limited and the aggregate stabilizes at a certain size. In literature the interaction between tails and heads is often neglected. The choice $\chi_{AB} = 1.5$ mimics a repulsion between these types of segments. If this interaction is too weak, the head groups mix too easily with tail segments and consequently too many tail segments would be exposed to the water phase. In this case no stable associates are formed. In the RIS scheme one extra parameter is needed, namely the energy difference between a *gauche* and a *trans* configuration. We used a value of 1 kT at $T = 275$. This resembles a literature value of around 0.8 kT at room temperature.[12]

Branch points

We have allowed minor simplifications with respect to the computations at the branch point. We will only account for nonoverlapping chain parts. In other words, a second order Markov approximation is used instead of a third order (RIS) Markov approximation. Typically, a second order Markov approximation has a chain end distribution function $G(z,s_1^{\alpha})$ which states that the free bond 2 will be connected with a segment in direction α, while bond 1 is connected with a chain in any of the three remaining directions. In this case all $\lambda^{\alpha''-\beta''-\gamma''\delta''}$ equal one-third for all possible combinations of the three meeting chain parts. Further, we did not distinguish between the two enantiomers. Consequently, the number of ways to connect the three subchains in the branch point is doubled. Therefore, in this case the normalization given in Eq. (14) for the branch segment $\lambda^{\alpha\beta\gamma} = \frac{1}{2}\lambda^{\alpha\beta}$ is used. In this way the number of operations for the branch point is reduced from 12 to 3.

Membrane in a frame

Membranes in a frame are known as black lipid films. Since they are restricted from translation, they are relatively easily examined experimentally. The membrane thickness and, more generally, the membrane composition can be modified by suitable experimental conditions. In our theory the membrane composition is changed by changing the lipid concentration in the system. In doing so, thermodynamic data can be calculated. Figure 3(a) shows how the excess free energy A^{σ} expressed as

$$A^{\sigma}/kTL = -\sum_i \frac{\theta_i^{\sigma}}{r_i} + \sum_z \ln \frac{\phi_W(z)}{\phi_W^b} + \frac{1}{2}\sum_z \sum_x \sum_y (\chi_{xW} + \chi_{yW} - \chi_{xy}) \times [\phi_x(z)\langle\phi_y(z)\rangle - \phi_x^b \phi_y^b] \tag{17}$$

depends, among other quantities, on the excess amount of lipid, θ_2^{σ}, which is a measure of the membrane thickness:

$$\theta_2^{\sigma} = \sum_{z=1}^{M} [\phi_2(z) - \phi_2^b] \, . \tag{18}$$

Figure 3(b) gives the equilibrium concentration of lipids in solution as a function of θ_2^{σ}. For very thin membranes the equilibrium concentration of lipids in the bulk (and hence their chemical potential) is high, but passes a minimum when the membranes grow thicker. A second minimum is present at high θ_2^{σ}, when on the membrane a second bilayer is formed (only present if the bilayers attract each other). In Fig. 3(a), the excess free energy of the film is behaving oppo-

Downloaded 28 Feb 2012 to 137.224.252.10. Redistribution subject to AIP license or copyright; see http://jcp.aip.org/about/rights_and_permissions

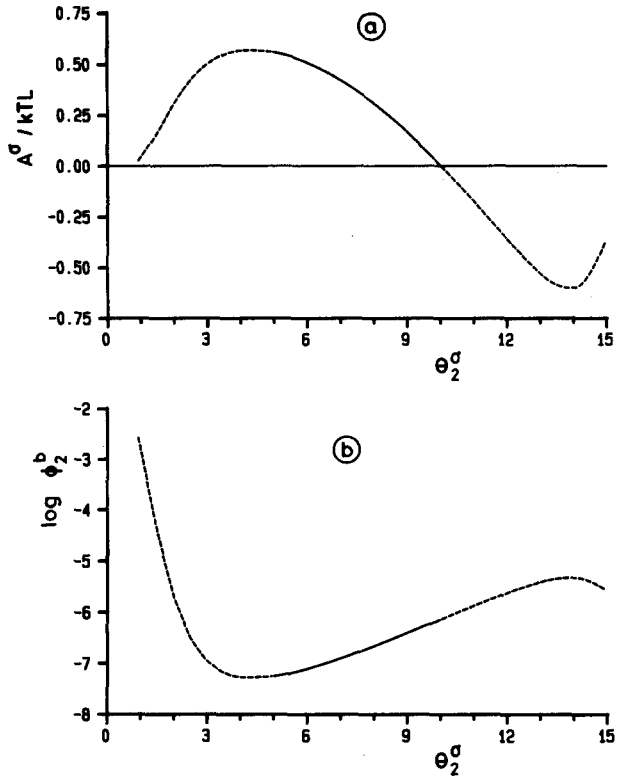

FIG. 3. (a) Excess surface free energy per lattice site as a function of θ_2^σ ("membrane thickness"). (b) Equilibrium volume fraction of lipids in the bulk as a function of θ_2^σ. The lipid membrane is composed of lecithin-like molecules of tail length 14 and head group size 3 (see the text). The solid parts of the curves represent stable membranes. Energy parameters: $\chi_{AW} = 1.6$; $\chi_{BW} = -0.3$; $\chi_{AB} = 1.5$; $U^s = 275/300\ kT$. Temperature: 300 K.

sitely: when the chemical potential decreases, the excess free energy increases. This is in accordance with Gibbs' law.

Only the middle part of the curves (solid lines) in Figs. 3(a) and 3(b) are operational. If A^σ is negative the membrane will spontaneously increase its surface area and thin membranes are unstable because $\partial A^\sigma/\partial\theta_2^\sigma > 0$ (see below).

Free membranes

In contrast with a membrane in a frame, a free membrane does not feel the constraint of the frame and therefore it will adjust its surface area A_s until the surface tension vanishes. From thermodynamics the change in Gibbs energy A at constant pressure p and temperature T, surface tension γ and chemical potential μ_i is

$$dA = \gamma dA_s + \sum_i \mu_i\, dn_i. \tag{19}$$

Indeed, equilibrium is established when $(\partial A/\partial A_s)_{p,T,n_i} = 0$, thus, $\gamma = 0$. For stable equilibrium the free energy A as a function of the area must be convex at this point: $(\partial A^2/\partial^2 A_s)_{p,T,n_i} > 0$, thus $(\partial\gamma/\partial A_s)_{p,T,n_i} > 0$. Since

$$\frac{\partial\theta_2^\sigma}{\partial A_s} < 0, \tag{20}$$

stable equilibrium is found when $(\partial\gamma/\partial\theta_2^\sigma) < 0$, or equivalently,

$$\frac{\partial(A^\sigma/L)}{\partial\theta_2^\sigma} < 0. \tag{21}$$

The stable points for the free membranes and the stability range for membranes in a frame are found with the help of Fig. 3(a).

The conclusion that free membranes have no surface tension is also reached by applying the thermodynamics of small systems,[13,14] assuming that the membrane has no translational entropy. Indeed, the translational entropy of the membrane is relatively small, but there are contributions due to undulations. The number of undulations and their distribution depend on the free energy of curvature of the bilayer. Curved bilayers (vesicles) will be examined in a following publication.[15] The wavelength of the undulations, is large compared to the membrane thickness, so that only a very small excess free energy per surface site is present. Therefore, all membrane systems discussed below are assumed to have a zero excess free energy.

First order Markov chains compared to rotational isomeric state scheme

Figure 4 shows the overall segment density profiles through a cross section of membranes consisting of lecithin molecules with tails of 14 segments. In Fig. 4(a) the first order Markov approximation is used, whereas in Fig. 4(b) the result for the RIS scheme is shown. The difference between the two graphs is obvious. As expected, the RIS scheme leads to considerably thicker membranes. As the chain density in the membranes is the same for both approximations, the head group density for the RIS membrane is higher. Nevertheless, the head group density is still rather low and therefore many tail segments are in contact with the water phase.

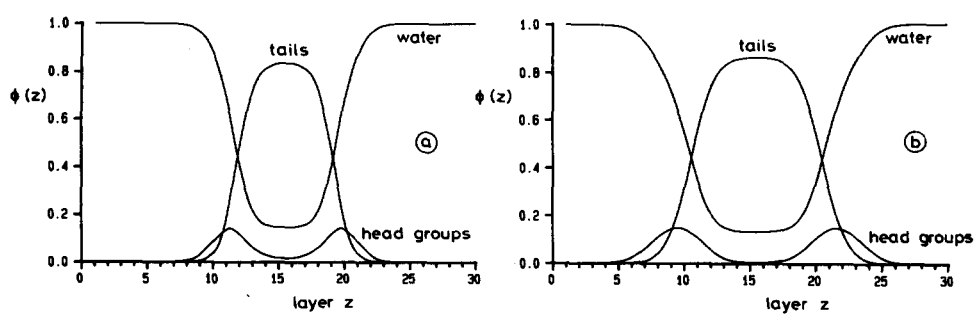

FIG. 4. Segment density profiles through cross sections of a membrane composed of lecithin-like molecules. Parameters as in Fig. 3. The layers are numbered arbitrarily. (a) First order Markov approximation. (b) RIS approximation.

Downloaded 28 Feb 2012 to 137.224.252.10. Redistribution subject to AIP license or copyright; see http://jcp.aip.org/about/rights_and_permissions

Figures 4(a) and 4(b) suggest that a large amount of water is present in the membrane, which is certainly an overestimation. The water concentration in the membrane reaches the binodal concentrations predicted by the Flory–Huggins (FH) theory.[16] It is well known that the FH theory (and hence also our theory) successfully predicts phase separation qualitatively, but that the compositions of the phases are wrong. Corrections for this defect are rather involved. One very successful method to improve the membrane picture will be discussed in a future publication where an orientation-dependent molecular field is introduced in the theory.[17] The model also needs to be improved with respect to the water phase (water molecules are treated as unpolarizable monomers). Further, a more advanced description of the membrane system must include the compressibility of the system. A full analysis of these last two factors is also left for future work.

RIS membranes

Figure 5 shows the segment density profiles of the lipids from Fig. 4(b) on a logarithmic scale for the volume fractions. In this figure we see that the segment density profiles outside the membrane fall off more or less exponentially until the bulk volume fraction is reached. This takes place over a distance comparable with the tail length of the lipids and with the membrane thickness. Apparently, very few dangling tails stick out of the membrane.

Our membranes are symmetrical with respect to the midplane, but the overall symmetrical segment density profile is composed of two asymmetrical contributions: one from each side of the membrane. We define a molecule to belong to that side of the membrane where the branching segment is found. Figure 6 shows the individual segment distributions in the membrane of Fig. 4(b). For every segment either the left-hand or the right-hand side profile is shown. Figure 6(a) represents tail number 1, Fig. 6(b) tail number 2, (closest to the head group) and Fig. 6(c) the glycerol backbone and the head group [see Eq. (16)]. All segments have a wide distribution, although segments in the glycerol backbone are confined to less layers than those in the molecular extremities (the two tail ends and the end of the head group). These results suggest that the glycerol backbone is the most rigid part of the molecule. Note that this rigidity is not due to intrinsic sterical hindrances inside the molecule itself but to interactions with the environment. Interestingly, the first tail (the one further away from the head group) is buried about half a layer deeper in the membrane than the tail next to the head group, and its segments have slightly wider distributions [compare Figs. 6(a) and 6(b)]. Clearly, the head group pulls the molecule towards the water phase and the tail closest to this head group is affected most. Similar trends are observed experimentally.[18]

Figure 7 gives θ_2^g as a function of the tail length p, for both first order Markov and RIS scheme calculations. Clearly, the RIS scheme produces thicker membranes and a larger increase in thickness per added tail segment. The membrane thickness is actually larger than θ_2^g, because the volume fraction of segments in the membrane is less than 1. The membranes found by our theory are about 50% too thin compared to experimental values.[19] (Other definitions of the membrane thickness can be given, which give up to 20% larger values.) One of the main reasons for this discrepancy is that in our approach the excluded volume of neighboring chains is only weakly incorporated. The tails bend too easily. In a future publication we will correct for this.[17] Other theor-

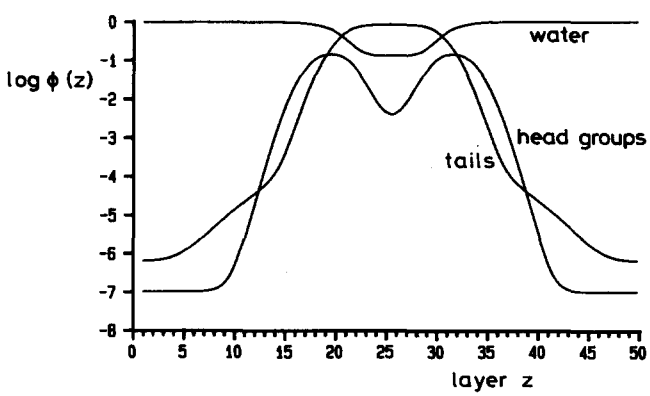

FIG. 5. Density profiles of the lipids of the membrane of Fig. 4(b) on a logarithmic scale for the volume fractions.

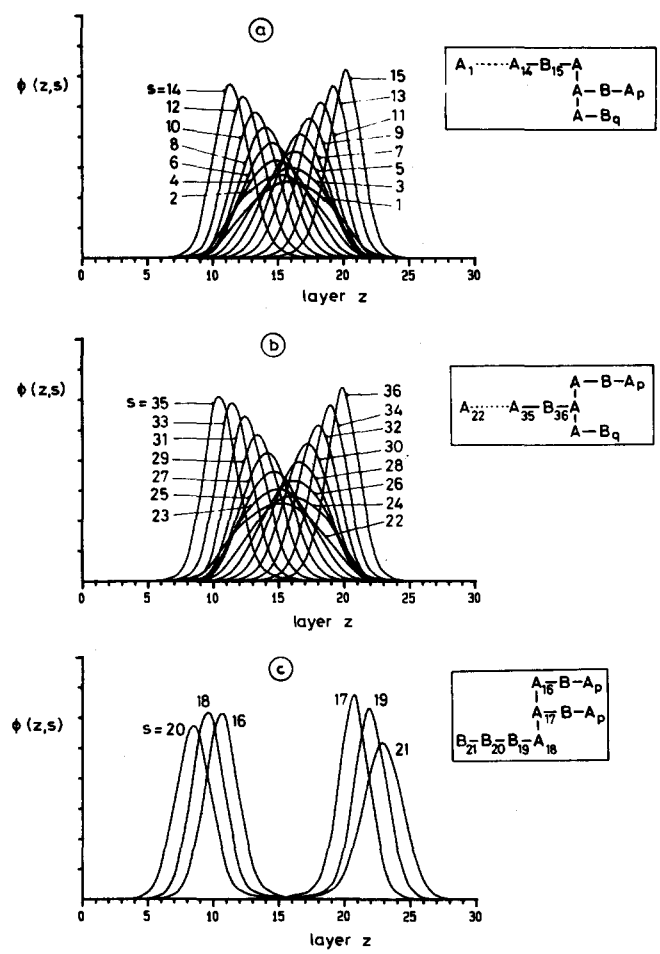

FIG. 6. Individual segment density profiles (in arbitrary units) for the membrane given in Fig. 4(b). The segment numbers are indicated [see Eq. (16)]. Only one side of each distribution is given. Details are given in the text.

Downloaded 28 Feb 2012 to 137.224.252.10. Redistribution subject to AIP license or copyright; see http://jcp.aip.org/about/rights_and_permissions

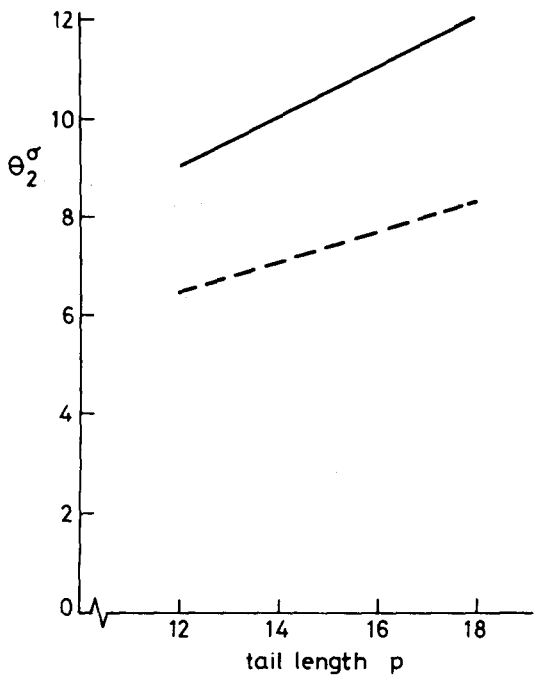

FIG. 7. Membrane thickness as a function of tail length of the lecithin molecules. Dashed line: first order Markov approximation, solid line: RIS Markov approximation. Energy parameters as in Fig. 3. Short molecules do not form membranes.

ies, which fix the head group density in a given plane, actually force the chains to do steps towards the center of the membrane, and therefore do not suffer from this problem, though at the expense of other (severe) simplifications.

Qualitatively, the results of Fig. 7 correspond with measurements reported by Cornell and Separovic.[19] Their conclusion, that a change in length of the acyl chain gives a smaller change in membrane thickness, is fully supported by our calculations. Their measurements indicate also, in accordance with our predictions, that in the center of the membrane the segments must have a more isotropic distribution. Quantitatively, our results overestimate this behavior, as explained above.

For surfactants (amphiphilic molecules with one apolar tail and a polar head group) often a linear relation between $\log(\phi_2^b)$ ($\approx$log CMC) and the number of apolar tail segments is found: $\log(\phi_2^b) = up + v$, where p is the number of tail segments, u the slope, and v the intercept.[20] Our calculations also show this linearity. Data for u and v are collected in Table III for various values of the four parameters in the model. The calculations are performed with the RIS scheme, but the first order Markov approximation gives similar trends. Inspection of Table III reveals that for the slope u only the interaction χ_{AW} between tails and solvent is important. The intercept is influenced by all parameters, but the head solvent interaction is most effective.

Table IV collects data for the dependence of θ_2^σ, a measure for the membrane thickness, on the energy parameters for a lecithin molecule with tail lengths of 16 segments and head group size $q = 3$. As can be seen in Table IV, the thickness increases when the interaction between tails and water becomes less favorable (χ_{AW} higher), when the head groups and water attraction is less (χ_{BW} less negative) and when the interaction between tails and head groups becomes smaller (χ_{AB} lower). The membrane thickness also increases if the stiffness of the chains increases. The energy parameters can only be chosen between certain limits: if, e.g., the head tail repulsion is too weak, no membranes exist for which the excess free energy is vanishing. Fitting the calculations with experimental values, especially critical micellisation concentration data, will give an indication of the values for the energy parameters.

CONCLUSIONS

The elegance of the present theory is that only four measurable energy parameters are needed to model the association behavior of lipid molecules to form membrane-like structures, without the need to restrict the head groups to given layers. Real equilibrium with a bulk solution is maintained. The Markov chain approximation allows for a very efficient generation of the set of conformations which can be calculated with standard numerical techniques in about 60 s on a VAX 8600 computer. The extension of the Markov statistics to the rotational isomeric state scheme improves the model considerably, as direct backfolding is excluded. The theory gives good insight into the force balance of the membrane. Some membrane properties found are not yet in full agreement with experiments, but the theory is easily improved and can be readily adopted to a wide range of complicated systems.

TABLE III. Dependence of $\log \phi_2^b = up + v$ on the energy parameters for lecithin molecules with $q = 3$ head group segments.

χ_{AW}	χ_{BW}	χ_{AB}	$U^g(kT)$	u	v
1.7	−0.3	1.5	275/300	−0.3186	1.745
1.6	−0.3	1.5	275/300	−0.2803	1.711
1.5	−0.3	1.5	275/300	−0.2426	1.656
1.6	−0.2	1.5	275/300	−0.2802	1.622
1.6	−0.4	1.5	275/300	−0.2804	1.799
1.6	−0.3	1.4	275/300	−0.2803	1.646
1.6	−0.3	1.6	275/300	−0.2803	1.775
1.6	−0.3	1.5	250/300	−0.2800	1.715
1.6	−0.3	1.5	300/300	−0.2806	1.708

TABLE IV. Dependence of the membrane thickness on the energy parameters for lecithin molecules with $p = 16$ and $q = 3$.

χ_{AW}	χ_{BW}	χ_{AB}	$U^g(kT)$	θ_2^σ
1.5	−0.3	1.5	275/300	10.31
1.6	−0.3	1.5	275/300	11.01
1.7	−0.3	1.5	275/300	11.66
1.6	−0.2	1.5	275/300	11.18
1.6	−0.4	1.5	275/300	10.86
1.6	−0.3	1.4	275/300	11.12
1.6	−0.3	1.6	275/300	10.92
1.6	−0.3	1.5	250/300	10.87
1.6	−0.3	1.5	300/300	11.16

Downloaded 28 Feb 2012 to 137.224.252.10. Redistribution subject to AIP license or copyright; see http://jcp.aip.org/about/rights_and_permissions

ACKNOWLEDGMENTS

The work of F. A. M. L. is part of the research program of the Stichting Scheikundig Onderzoek Nederland (S. O. N.), which is financially supported by the Nederlandse Organisatie voor Wetenschappelijk Onderzoek (N. W. O).

APPENDIX A

Referring to Table II, Eq. (2a) is written in the form

$$\mathbf{G}(z,s_1) = \mathbf{G}(z,s) \sum_{z'} \boldsymbol{\lambda}_{z'-z} \mathbf{G}(z',s_1'), \tag{A1}$$

where

$$\mathbf{G}(z,s) = \begin{bmatrix} G(z,s^{eh}) & 0 & 0 & 0 & 0 & 0 & 0 \\ 0 & G(z,s^{ef}) & 0 & 0 & 0 & 0 & 0 \\ 0 & 0 & G(z,s^{fh}) & 0 & 0 & 0 & 0 \\ 0 & 0 & 0 & G(z,s^{fg}) & 0 & 0 & 0 \\ 0 & 0 & 0 & 0 & G(z,s^{fe}) & 0 & 0 \\ 0 & 0 & 0 & 0 & 0 & G(z,s^{hf}) & 0 \\ 0 & 0 & 0 & 0 & 0 & 0 & G(z,s^{he}) \end{bmatrix} \tag{A2}$$

and

$$\boldsymbol{\lambda}_{-1} = \begin{bmatrix} \lambda^t & 0 & 2\lambda^g & 0 & 0 & 0 & 0 \\ \lambda^g & 0 & \lambda^t+\lambda^g & 0 & 0 & 0 & 0 \\ 0 & 0 & 0 & 0 & 0 & 0 & 0 \\ 0 & 0 & 0 & 0 & 0 & 0 & 0 \\ 0 & 0 & 0 & 0 & 0 & 0 & 0 \\ 0 & 0 & 0 & 0 & 0 & 0 & 0 \\ 0 & 0 & 0 & 0 & 0 & 0 & 0 \end{bmatrix}, \quad \boldsymbol{\lambda}_1 = \begin{bmatrix} 0 & 0 & 0 & 0 & 0 & 0 & 0 \\ 0 & 0 & 0 & 0 & 0 & 0 & 0 \\ 0 & 0 & 0 & 0 & 0 & 0 & 0 \\ 0 & 0 & 0 & 0 & 0 & 0 & 0 \\ 0 & 0 & 0 & 0 & 0 & 0 & 0 \\ 0 & 0 & 0 & 0 & \lambda^t+\lambda^g & 0 & \lambda^g \\ 0 & 0 & 0 & 0 & 2\lambda^g & 0 & \lambda^t \end{bmatrix},$$

$$\boldsymbol{\lambda}_0 = \begin{bmatrix} 0 & 0 & 0 & 0 & 0 & 0 & 0 \\ 0 & 0 & 0 & 0 & 0 & 0 & 0 \\ 0 & \lambda^t & 0 & \lambda^g & 0 & \lambda^g & 0 \\ 0 & \lambda^g & 0 & \lambda^t & 0 & \lambda^g & 0 \\ 0 & \lambda^g & 0 & \lambda^g & 0 & \lambda^t & 0 \\ 0 & 0 & 0 & 0 & 0 & 0 & 0 \\ 0 & 0 & 0 & 0 & 0 & 0 & 0 \end{bmatrix}, \quad \mathbf{G}(z,s_1) = \begin{bmatrix} G(z,s_1^{eh}) \\ G(z,s_1^{ef}) \\ G(z,s_1^{fh}) \\ G(z,s_1^{fg}) \\ G(z,s_1^{fe}) \\ G(z,s_1^{hf}) \\ G(z,s_1^{he}) \end{bmatrix}. \tag{A3}$$

The equivalent Eq. (A1) for evaluating the chain end distribution functions from the opposite chain end reads

$$\mathbf{G}(z,s_2) = \mathbf{G}(z,s) \sum_{z'} \mathbf{X}\boldsymbol{\lambda}_{z'-z}\mathbf{X}\mathbf{G}(z',s_2'), \tag{A4}$$

where the product $\mathbf{X}\boldsymbol{\lambda}\mathbf{X}$ is a $\boldsymbol{\lambda}$ matrix that operates on bond 1 of segment s', instead of bond 2. The matrix X rearranges the segment orientations, so that orientation $\alpha\beta$ replaces $\beta\alpha$, and is given by

$$\mathbf{X} = \begin{bmatrix} 0 & 0 & 0 & 0 & 0 & 0 & 1 \\ 0 & 0 & 0 & 0 & 1 & 0 & 0 \\ 0 & 0 & 0 & 0 & 0 & 1 & 0 \\ 0 & 0 & 0 & 1 & 0 & 0 & 0 \\ 0 & 1 & 0 & 0 & 0 & 0 & 0 \\ 0 & 0 & 1 & 0 & 0 & 0 & 0 \\ 1 & 0 & 0 & 0 & 0 & 0 & 0 \end{bmatrix}. \tag{A5}$$

The volume fractions are calculated with [see Eqs. (4a) and (14)]

$$G(z,s_{12}) = \mathbf{G}^T(z,s_1)\mathbf{G}^{-1}(z,s)\mathbf{W}\mathbf{G}(z,s_2) \tag{A6}$$

after suitable normalization. In Eq. (A6),

$$\mathbf{W} = \frac{1}{12}\begin{bmatrix} 1 & 0 & 0 & 0 & 0 & 0 & 0 \\ 0 & 2 & 0 & 0 & 0 & 0 & 0 \\ 0 & 0 & 2 & 0 & 0 & 0 & 0 \\ 0 & 0 & 0 & 2 & 0 & 0 & 0 \\ 0 & 0 & 0 & 0 & 2 & 0 & 0 \\ 0 & 0 & 0 & 0 & 0 & 2 & 0 \\ 0 & 0 & 0 & 0 & 0 & 0 & 1 \end{bmatrix}. \tag{A7}$$

Alternatively, one can use the same $\boldsymbol{\lambda}$ matrices as given in Eq. (A3), but then the vectors G are replaced by vectors XG and the matrix G by XGX. The equivalent Eq. (A4) reads

$$\mathbf{X}\mathbf{G}(z,s_2) = [\mathbf{X}\mathbf{G}(z,s)\mathbf{X}] \sum_{z'} \boldsymbol{\lambda}_{z'-z} [\mathbf{X}\mathbf{G}(z,s_2')]. \tag{A4a}$$

When there is no preferential orientation of a monomer then

Downloaded 28 Feb 2012 to 137.224.252.10. Redistribution subject to AIP license or copyright; see http://jcp.aip.org/about/rights_and_permissions

$\mathbf{XGX} = \mathbf{G}$. Equation (A6) becomes

$$G(z,s_{12}) = \mathbf{G}^T(z,s_1)\mathbf{G}^{-1}(z,s)\mathbf{WX}[\mathbf{XG}(z,s_2)]. \quad \text{(A6a)}$$

Equations (A6) and (A6a) are identical because the product XX gives the identity matrix.

APPENDIX B

The volume fraction profiles cannot be found analytically. We have an implicit set of equations which can be solved, for instance, with the FORTRAN program of Powell.[21] If we formulate the k th guess for the free segment weighting factors as $G_x^{(k)}(z)$, then

$$-u_x'(z)/kT = \ln[G_x^{(k)}(z)] - \sum_y \chi_{xy}\left(\frac{\langle\phi_y(z)\rangle}{\Sigma_{y'}\phi_{y'}(z)} - \phi_y^b\right). \quad \text{(B1)}$$

The volume fractions $\phi_x(z)$ are obtained from $G_x^{(k)}(z)$ and normalized by $\theta_i/[r_i G_i(r_1)]$ except for the solvent profile, for which we use $\phi_1^b = 1 - \Sigma_{i\neq 1}\phi_i^b = 1 - \Sigma_{i\neq 1}\theta_i/[G_i(r_1)]$. The denominator $\Sigma_{y'}\phi_{y'}(z)$ is the sum of volume fractions in layer z and is introduced to avoid too strong fluctuations of $u_x'(z)$ during the iterations. It will be 1 when the final solution is attained. Further, we define

$$u'(z) = \frac{1}{\Sigma_y 1}\sum_y u_y'(z) \quad \text{(B2)}$$

as the average $u'(z)$. The boundary conditions are

$$\sum_y \phi_y(z) = 1 \quad \text{(B3)}$$

and

$$u_x'(z) = u'(z) \quad \text{(for all segment types } x\text{)}. \quad \text{(B4)}$$

The following function can be formulated which combines all requirements:

$$f_x(z) = 1 - \frac{1}{\Sigma_y\phi_y(z)} + u'(z) - u_x'(z). \quad \text{(B5)}$$

This function is reasonably linear in $G_x^{(k)}(z)$ and only zero for all x and z when Eqs. (B3) and (B4) are obeyed.

The iteration is started by a small (step) profile in the free segment weighting factors to initiate inhomogeneities near the reflecting boundary. The tolerance $\sqrt{[\Sigma_z\Sigma_x f_x(z)^2]}$ was typically less than 10^{-8}.

[1] F. A. M. Leermakers, J. M. H. M. Scheutjens, and J. Lyklema, Biophys. Chem. **19**, 352 (1983).
[2] P. van der Ploeg and H. J. C. Berendsen, J. Chem. Phys. **76**, 3271 (1982).
[3] H. J. C. Berendsen and B. Egberts J. Chem. Phys. (in press).
[4] B. Jönsson, O. Edholm, and O. Teleman, J. Chem. Phys. **85**, 2259 (1986).
[5] B. Owenson and L. R. Pratt, J. Phys. Chem. **88**, 2965 (1984).
[6] I. Szleifer, A. Ben-Shaul, and W. M. Gelbart, J. Chem. Phys. **85**, 5345 (1986).
[7] D. W. R. Gruen, J. Phys. Chem. **89**, 153 (1985).
[8] K. A. Dill and R. S. Cantor, Macromolecules **17**, 380 (1983).
[9] F. A. M. Leermakers, P. P. A. M. van der Schoot, J. M. H. M. Scheutjens, and J. Lyklema, in *Surfactants in Solution. Modern Applications*, edited by K. L. Mittal (in press).
[10] J. M. H. M. Scheutjens, and G. J. Fleer, J. Phys. Chem. **83**, 1619 (1979).
[11] E. A. Di Marzio and R. J. Rubin, J. Chem. Phys. **55**, 4318 (1971).
[12] N. K. Adam and G. Jessop, Proc. R. Soc. London Ser. A **112**, 362 (1926).
[13] D. G. Hall and B. A. Pethica, in *Nonionic Surfactants*, edited by M. J. Schick (Marcel Dekker, New York, 1976), Chap. 16.
[14] T. L. Hill, *Thermodynamics of Small Systems* (Benjamin, New York, 1963, 1964), Vols. 1 and 2.
[15] F. A. M. Leermakers and J. M. H. M. Scheutjens, J. Phys. Chem. (submitted).
[16] P. J. Flory, *Principles of Polymer Chemistry* (Cornell University, Ithaca, NY, 1953).
[17] F. A. M. Leermakers and J. M. H. M. Scheutjens, J. Phys. Chem. (submitted).
[18] G. Büldt, H. U. Gally, A. Seelig, and J. Seelig, Nature **271**, 183 (1978).
[19] B. A. Cornell and F. Separovic, Biochem. Biophys. Acta **733**, 189 (1983).
[20] C. Tanford, *The Hydrophobic Effect: Formation of Micelles and Biological Membranes* (Wiley, New York, 1973).
[21] M. J. D. Powell, in *Numerical Methods for Nonlinear Algebraic Equations*, edited by P. Rabinowitz (Gordon and Breach, London, 1970), p. 115.

Downloaded 28 Feb 2012 to 137.224.252.10. Redistribution subject to AIP license or copyright; see http://jcp.aip.org/about/rights_and_permissions